Advances in Water Resources 32 (2009) 1717–1725

Contents lists available at ScienceDirect

Advances in Water Resources

journal homepage: www.elsevier.com/locate/advwatres

Mean flow and turbulence around experimental spur dike

Jennifer G. Duan [a,*], Li He [a,b], Xudong Fu [b], Quangqian Wang [b]

[a] Department of Civil Engineering, University of Arizona, 1209 E. 2nd Street, Tucson, AZ 85721, United States
[b] State Key Lab of Hydroscience and Engineering, Department of Hydraulic Engineering, Tsinghua University, Beijing, P.R. China

ARTICLE INFO

Article history:
Received 8 October 2008
Received in revised form 6 September 2009
Accepted 7 September 2009
Available online 20 September 2009

Keywords:
microADV
Mean flow
Spur dike
Turbulence

ABSTRACT

An acoustic Doppler velocimeter was used to measure flow and turbulence around an experimental spur dike in a flat and a scoured bed. Differences of mean velocity, turbulent intensity and Reynolds stresses between these two flow fields were analyzed. Upon the formation of scour hole, mean flow velocities in the downstream and lateral directions were reduced, but increased in the vertical direction. The turbulence intensities (u' and v') are much larger, and the vertical component (w') is smaller than that in the flat bed. Among three Reynolds stresses, the $-\rho\overline{u'w'}$ and $-\rho\overline{v'w'}$ components are much smaller than the $-\rho\overline{u'v'}$. Bed shear stress near the dike can be 6 to 8 times as large as that of the approaching flow so that a local scour is developed near the dike without the shear stress of approaching flow exceeding the critical shear stress of bed material. The local scour initiated at the upstream of the dike and then extends to downstream from the dike tip. These results indicated that the development of local scour synchronizes to high shear stresses resulted from the horseshoe vorticies on a mobile bed surface.

1. Introduction

Spur dikes are hydraulic engineering structures for preserving the desired water depth, deflecting the main current in the harbor channels and rivers, and protecting river banks. Flow field passing through a spur dike is characterized with the separation of approaching flow in three dimensions (3D) from upstream to the horseshoe vortex downstream of the dike [2]. The complexity of flow field increases as the scour hole develops [11,20].

Local scour is caused by the erosive forces from flow turbulence acting on the erodible bed in the vicinity of an obstacle or structure placed in a stream, such as a spur dike, or bridge pier. Mean flow and turbulence properties are equally important for sediment entrainment, suspension, transportation, and deposition [6]. The scour mechanism involves two interactive elements, one is 3D unsteady flow field near the boundary, especially turbulent fluctuations and the resultant bed shear stresses; and the other is the morphology of sediment particles on bed surface [6,22]. The transport of sediment particles in turbulent flows depends on the interactions between the particles and the coherent turbulent structures [9]. Bey et al. [6] found turbulence fluctuations other than mean flow features directly influence the scour process.

Mean bed-shear stress or near-bed velocity were traditionally used for estimating the rate of sediment transport in well developed boundary layer flows [23,26,36,38]. For flows with developing boundary layers of sufficient non-uniform topography or roughness, sediment transport does not directly correlate to mean flow properties [27]. Research found near-bed turbulence structure played a significant role in transporting sediment through a combination of microADV, LDV, PIV and high-speed motion picture photography measurements [27,28]. Recent measurements found that hydraulic forces acting on various sized sediment particles vary according to bed configurations [33]. Measured turbulent flow field (e.g., turbulence intensities, Reynolds shear stresses) at various azimuthal planes around a 45° wing-wall and vertical-wall abutment concluded that the near-bed Reynolds stresses are more accurate for estimating sediment transport rate [10,11]. Sterk et al. [35] found normal Reynolds stresses ($\rho\overline{u'^2}$ and $\rho\overline{w'^2}$) contributed more than the Reynolds stresses $-\rho\overline{u'w'}$ to sand transported by saltation in two-dimensional flows. Experiments of Nelson et al. [27] and Wu and Jiang [38] both showed that $-\rho\overline{u'w'}$ poorly correlates to sediment entrainment in turbulent boundary layers, however turbulent bursts by u' and w' components played a significant role in producing shear stresses. Normal stress $\rho\overline{u'^2}$ is a better predictor for the entrainment of coarse sand and gravels than $\rho\overline{w'^2}$ and $-\rho\overline{u'w'}$ in 2D flows because there was a strong positive correlation between the transport rate and near-bed instantaneous streamwise velocity [8,27,29]. The most effective events that move sediment are those with a large u'. Therefore, sediment flux can increase even when bed shear stress decreases [27]. Applying concepts derived from steady uniform flow to non-uniform flows of developing boundary layer are problematic [17,27].

* Corresponding author. Tel.: +1 520 626 5946.
E-mail address: gduan@email.arizona.edu (J.G. Duan).

0309-1708/$ - see front matter © 2009 Elsevier Ltd. All rights reserved.
doi:10.1016/j.advwatres.2009.09.004

Nomenclature

B	width of flume
h	depth of flow
L	length of dike
Re	Reynolds number
u_j, v_j, w_j	instantaneous velocity components in x, y and z direction
u', v', w'	velocity fluctuation in x, y and z direction; Reynolds-decomposed velocity fluctuation
u_0	approaching flow velocity
u_*	shear velocity, friction velocity
x, y, z	longitudinal, transverse and vertical directions, namely streamwise, lateral and bed-normal co-ordinates
ρ	mass density of fluid
τ_0	bed-shear stress of approaching flow, ρu_*^2
τ_b	bed-shear stress
n	the ensemble size of velocity measurement at one measuring point
δ	thickness of viscous sublayer
Subscript	
j	the velocity measurement at one point

Two- and three-dimensional simulations of flow fields around spur dikes have been reported intensively in the literature. Two-dimensional (2D) depth-averaged models [16,19,37] have been used to simulate hydrodynamic flow fields near dikes by including corrections for streamline curvature in momentum equations. Duan and Nanda [16] applied an enhanced 2D model [13–15] to study suspended sediment transport in a multiple-groyne field within a natural river. Results from this study indicated that a 2D model can simulate approximately the horizontal recirculation and deposition of suspended sediment. Jia et al. [19] and Nagata et al. [26] employed a full three dimensional hydrodynamic model by solving the Reynolds-averaged Navier–Stokes equation to simulate flow field and sediment transport around a spur dike. All these models [7,19,21,26,31] were verified by measuring the time-averaged mean velocity field. Verifications regarding turbulence characteristics (e.g., turbulence intensity, normal stresses, Reynolds stresses) were limited due to lack of measurements. Therefore, to verify numerical models presently in use requires more reliable laboratory or field data of turbulence generated by flow around a dike or the evolution of turbulence passing through the dike.

The present experimental study aims to study mean and turbulence flow field in a flat and a scoured bed. Turbulent flow passing through an emergent spur dike on a flat and a scoured bed were measured, respectively, by using a SonTek 16-MHz MicroADV. Time histories of velocities in all three spatial dimensions were recorded at cross sections parallel to the dike. These measurements were used to study time-averaged, downstream primary flow and cross-sectional flow properties, as well as turbulence properties (e.g., turbulence intensities) at the upstream and downstream sections of the dike. Impacts of the dike on flow structure include flow convergence, locally increased bed-shear stress, and increased turbulence in the vertical, which explains the initiation of local scour and sorting of sediment in the scour hole.

2. Experimental data

2.1. Experiment set

Experiments were conducted in a 12.8-m long and 60.8-cm wide flume located at the St. Anthony Falls Laboratory, University of Minnesota. A valve was used to control discharge. The channel sides are glass walls, and bed slope was 0.0004. Bed surface had a roughness height about 0.4 mm. A 20-cm long, 4-mm thick, and 40-cm height metal plate was installed at 6 m downstream of the flume inlet and protruded from the right-hand side of the flume to serve as a model dike structure, and it emerged from the water surface during all experimental runs. Two experiments were performed: firstly channel bed was fixed; secondly, bed surface was covered with a well-sorted sand and gravel mixture having a median grain diameter of 1.59 mm.

A downward looking microADV was used to measure instantaneous velocity field. MicroADV has been commonly used in measuring point-wise 3D velocity fields through recording the Doppler shift produced by targeted material in the flow [12,20,32,34]. The acoustic sensor consisted of one transmitter and three receivers. The receivers are aligned to intersect with the transmit beam at a small sampling volume located about 50 mm from the probe tip. The sample volume is a cylinder of diameter 4.0 mm and height of 5.6 mm. The sampling volume of ADV is larger than those of Laser-based velocimetry (e.g. LDV, PIV). Blanckaert and McLelland [5] compared the accuracies of laser-based PIV and Acoustic Doppler Velocity Profiler and found that ADVP measured the turbulence accurately while PIV measurements of turbulence have the lower temporal resolution and the higher noise level. A recent near-bed turbulence measurement [30] showed that a typical size of sweep events contributing to bed load motion has a representative length of 0.8cm given the duration of 0.05 second and a celerity of 16 cm/s. This length is one time larger than that of a typical ADV sampling volume. This up-to-date literature [5,29] indicated acoustic Doppler velocimetry is accurate for measuring turbulence in open channel flows despite of its sampling volume. Even though more comparison studies of ADV and LDV (PIV) are expected to further verify these conclusions [5,29].

The sampling frequency of this ADV application was 25 Hz, with a sampling duration of 1 to 1.5 minutes in each measuring location. It can measure mean flow velocities from 1 mm/s to 2.5 m/s with an accuracy of ±1% of the measurement range. The microADV was attached to a point gauge fixed on an instrument carriage that was mounted on horizontal steel rails and moved on wheels. The ADV can move along the flume automatically driven by an electric motor, and also manually in the transverse and vertical directions to measure flow velocities at any location near the dike.

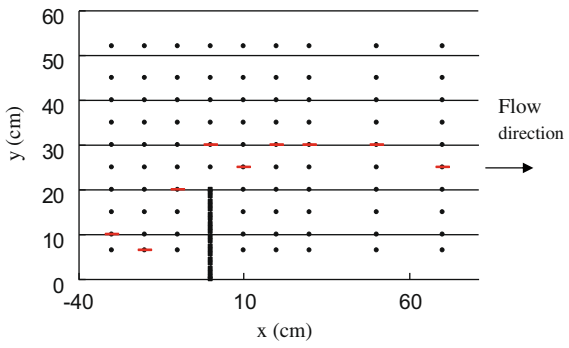

Fig. 1. Plan view of the experimental flume with measurement points denoted with solid dots, and red bars are the locations of thalweg at each cross section.

Nine cross sections shown in Fig. 1, including three upstream of the dike, one at the dike tip, and five downstream of the dike, were measured. Nine vertical profiles at intervals of 5 cm were measured at each cross section, and each vertical profile had 7–9 points with 1 cm spacing. At each measuring node, about 1500 instantaneous velocities at three respective directions were recorded. Flow depth was measured with a laser profiler attached to the instrument carriage at locations where velocity was measured. These measurements of velocities and surface elevations were used to determine mean velocities, turbulence intensities, Reynolds stresses, and bed-shear stresses. Hydraulic parameters for the present experiments are summarized in Table 1.

2.2. Data Processing

In the data analysis, the origin of the Cartesian coordinate is at the upstream side of the dike on the right wall of the initial bed surface elevation, thus the x-axis is the downstream direction, y-axis is pointing to the left bank in the transverse direction, and z-axis is towards the water surface in the vertical. The $z = 0$ plane was the flume bottom in the flat bed run, but the initial bed surface in the erodible bed run. The velocity components are denoted as u_j, v_j, and w_j, respectively.

The friction velocity of approaching flow was calculated by fitting the velocity profiles with the logarithmic law. Because of the effects of side wall the maximum mean velocity $\bar{u}$ occurred slightly below the free surface, indicative of the dip phenomenon [3] when an open channel flow had a low width to depth ratio ($B/H \leqslant 5$) [3,27,28]. The shear velocity, $u_* = 1.2$ cm/s, and zero velocity level, z_0, were determined by assuming the von Karman constant is 0.41. Flow is hydraulically rough with $ks = 1.20$ mm in the flat-bed runs. Whereas in the erodible bed run, the shear velocity was $u_* = 5.55$ cm/s and the roughness height was $ks = d_{50} = 1.59$ mm, which was much greater than the thickness of viscous sublayer $\delta = 11.6\frac{\nu}{u_*} = 0.234$ mm. The standard deviation of sediment mixture is 2.041. Therefore, flow in the erodible bed runs was also hydraulically rough. The mean velocity of approaching flow is 59.43 cm/s. Dey and Barbhuiya [11], Dey and Raikar [12], Duan et al. [13] and many others used dimensionless turbulence properties (e.g. turbulence intensity, TKE, shear stress) to generalize their distributions in fully developed turbulent flows. These measurements showed that when Reynolds number is over 10,000, the distributions of dimensionless turbulence intensities and bed shear stress are independent of approaching flows. At present, no convincing experimental evidences are available to verify if the results of dimensionless turbulence properties vary with the approaching flows at high Reynolds number. This study assumed the distributions of turbulence properties and bed shear stresses are typical for flows around a spur dike of flat and eroded bed surface because flows in both experiments are fully hydraulic rough with Reynolds number greater than 38,000.

At solid walls, all mean and turbulence velocities and Reynolds stresses are zero. Because of the complex turbulence flow near the dike, this study linearly interpolated these properties at each vertical line. The duration of the experimental run was 48 hours to allow the local scour reach an asymptotic state so that bed surface was completely armored. Contour lines of the scoured depth are shown in Fig. 2 in which the zero contour line is the initial bed surface and also the edge of the scouring hole. A photo of scoured bed surface is shown in Fig. 2b. The total scour volume was 0.0081 m^3. The maximum scour depth is 8.87 cm at $x = 15.4$ cm, $y = 25$ cm.

3. Results and discussion

3.1. Mean velocity

The contour lines of dimensionless time-averaged velocity components $\bar{u}, \bar{v}$ and $\bar{w}$ at different cross sections of the flat and scoured bed are shown in Fig. 3a and b, respectively. The distributions of downstream component of mean velocity are similar, but the distributions of lateral and vertical components of mean velocities are very different. In both cases the maximum downstream mean velocity occurred slightly below the free surface [4]. This dip phenomenon is noticeable because of the small flow aspect ratio in the present experiments [3]. The small channel aspect ratio together with the presence of free surface induces the secondary flow that dampens the vertical velocity fluctuations [3].

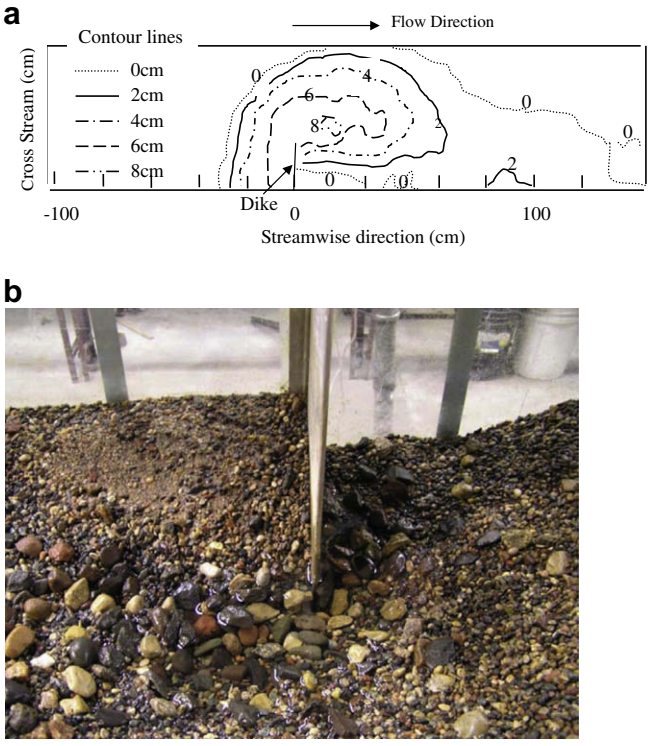

Fig. 2. (a) Plan view of contour lines of bed elevation in the scour hole. (b) Photo of scoured bed surface.

Table 1
Experimental data summary.

	Approaching velocity u_0 (cm/s)	Flow depth (cm)	B/H	Discharge (m^3/s)	Gradient	$\tau_0 = \rho u_*^2$ (Pa)
Eroded bed	59.43	16	3.75	0.058	0.0004	3.08
Flat bed	38.93	16	2.8	0.038	0.0004	0.144
	Shear velocity u_* (cm/s)	Thickness of viscous sublayer δ (mm)	Re ($\times 10^4$)	ks (mm)	Correlation parameter (R^2)	
Eroded bed	5.55	0.234	8.61	1.59	0.86	
Flat bed	1.2	1.08	3.89	1.20	0.94	

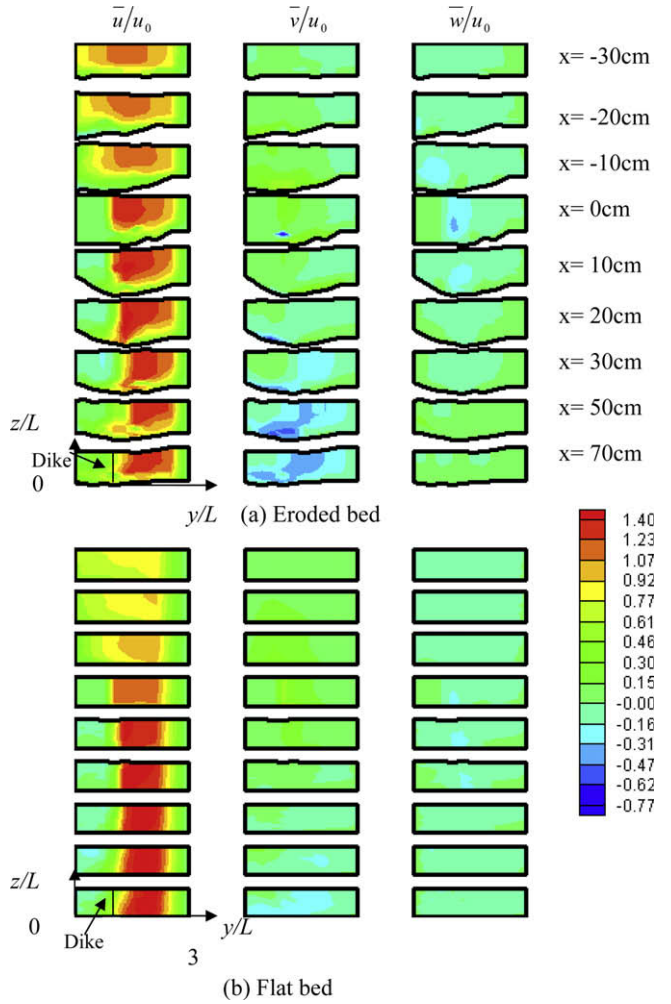

Fig. 3. Distribution of dimensionless mean velocities at cross sections for the scoured and flat bed surfaces ($\bar{u}/u_0, \bar{v}/u_0$ and $\bar{w}/u_0$) (u_0 is the approaching flow velocity).

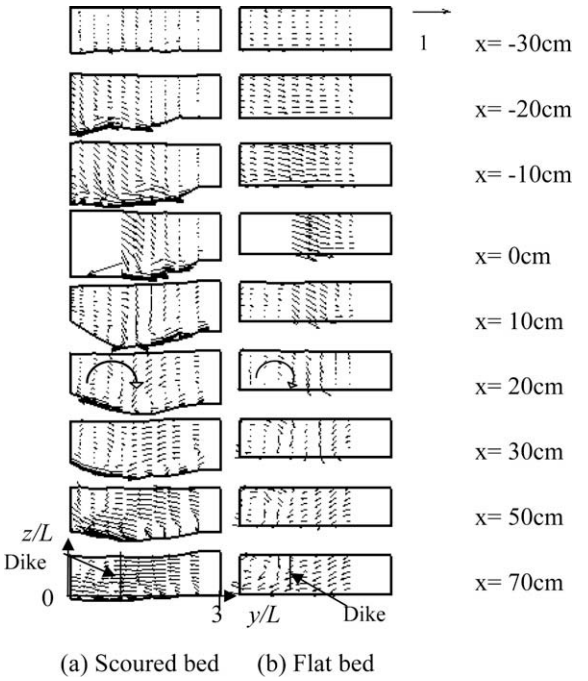

Fig. 4. Dimensionless velocity vector ($\bar{v}/u_0, \bar{w}/u_0$) at different cross sections.

Flow separation begins at the dike tip in both runs, and shifts slightly towards the right bank, and then turns back to the left side wall as shown in Fig. 4. The length of flow separation in the asymptotic state is about 3.5 times the dike length, much shorter than that for non-erodible flat bed. Flow reattached immediately at the end of the scour hole. The detached shear layer has nearly zero mean downstream velocity, and coincides with the thalweg of bed surface, especially at sections with $0.5 < x/L < 3.5$. One can find that the maximum scour depth developed along the path of the detached shear layer where the turbulence intensity is the maximum.

In the scoured bed, the mean velocity component, $\bar{u}$, at the contraction section is about 1.2 times as that of the mean velocity of approaching flow, while in the flat bed, the mean velocity at the contraction is about 1.3 times as that of the approaching flow. This shows that the streamwise component of mean velocity has been reduced after the scour hole is formed as observed by Thompson [37]. In the meantime, the downstream component of mean velocity near the bed was increased in the primary flow zone and reduced in the recirculation zone where negative velocities (in blue[1] color) are shown in Fig. 3a. The increase in $\bar{u}$ and the extent of recirculation zone are much larger in the flat bed than that in the scoured bed. However, the mean velocity of recirculating flow is less than 10% of the approaching flow velocity.

The mean downstream velocity, $\bar{u}$, reaches its maximum at the dike section in the scoured bed. The streamwise velocity has been greatly reduced in the scoured zone. At the zone above the initial bed where $z/L > 0.0$, the distribution of mean flow velocity is similar to that in the plane bed. Flow contracted at the dike section, and consequently the contour lines of $\bar{u}$ showed the existence of a pronounced skewness in the $\bar{u}$ component. This attributes to the effect of the horseshoe vortex and the associated helicoidal flow around the dike.

In both cases, the transverse component of mean velocity increases as flow approaches to the dike. At the dike section the transverse velocity in the primary flow reaches the maximum near the bed, and it is towards the left bank. The transverse velocity reverses its sign in the flow recirculation zone. The apparent difference in the distribution of $\bar{v}$ is that the maximum $\bar{v}$ in both the primary and the recirculation flows in the flat bed are larger than that in the scoured bed, which implies the reduction of flow intensity in the scour hole.

The mean vertical velocity, $\bar{w}$, approximately is zero at regions upstream of the dike influenced zone. As flow approaches the dike, the negative values of $\bar{w}$ upstream of the dike corroborate the existence of a strong downward flow in the scoured bed, while the mean vertical flow is upward at the tip of the dike in the flat bed. This phenomenon showed that the helicoidal flow originated at the dike tip in the flat bed has shifted to the upstream after the scour hole was formed. The magnitude of $\bar{w}$ decreases as the helicoidal flow attenuates downstream of the dike. The mean vertical velocity is the maximum at approximately the middle of flow depth and decreases towards both the surface and the bed. At $x/L = 5.0$, Fig. 3a shows a strong upward flow where hydraulic suction may take place that dislodges bed sediment downstream of the dike. Further downstream $\bar{w}$ diminishes rapidly.

In summary, for the scoured bed, the mean downstream velocity was reduced primarily due to the enlarged cross sections. On the other hand, the mean transverse velocity has increased near the bed surface in the scour hole, and the mean vertical velocity re-

[1] For interpretation of color in Figs. 1, 3 and 6–9, the reader is referred to the web version of this article.

verses its direction towards the flow surface in the scour hole. The increases in the lateral and vertical mean flow indicated sediment entrainment and transport towards the left bank.

3.2. Secondary flow

The time-averaged mean velocity vector $(\bar{v},\bar{w})$ in Fig. 4 formed the helicoidal flow at each cross section. Fig. 4 formed both the secondary flow and the downflow at the upstream face of the dike. In the scoured bed, the cross sectional circulation begins at the upstream of the dike, and gradually increases toward the dike until reaching its maximum at section $x/L = 1.0$, and then decreases gradually and disappears at section $x/L = 3.5$. The circulatory motion is relatively weak above the original bed surface, $z/L > 0.0$, but is stronger near the bed. Upstream of the dike the circulation is counter-clockwise at the dike section, and the one in the recirculation zone downstream of the dike is clockwise. As to the secondary flow in the flat bed, the circulatory motion in the scoured bed is weaker and constrained within the scoured zone, and its length is much shorter.

The dimensionless time-averaged mean velocity vector $(\bar{u},\bar{v})$ at different horizontal planes, $z = 0.1h, z = 0.5h$ and $z = h$, were shown in Fig. 5. Velocities at water surface were linearly interpolated from measured data. In the scoured bed, the recirculation flow behind the dike within the scour hole is weaker than that in the flat bed at the horizontal plane $z = 0.1h$. The recirculation flow in the scoured hole is very weak near the bed. As flow separates at the dike, the recirculation flow is stronger as it emerges towards water surface. Downstream of the dike at $z = 0.5h$, the width of flow separation zone keeps almost the same. In contrast, the horizontal recirculation in the flat bed remains almost the same regardless of its distance to the bed surface. The recirculation zone in the scoured bed is slightly smaller than that in the flat bed because the scoured bed surface is transporting sediment that dissipates more energy.

3.3. Turbulence Intensity

Reynolds decomposition into mean and fluctuating portions is commonly employed in analyzing turbulence velocity fields [1]. The contour lines of dimensionless turbulence intensities in 3D, symbolized as $\sqrt{\overline{u'^2}}/u_*, \sqrt{\overline{v'^2}}/u_*, \sqrt{\overline{w'^2}}/u_*$ at different cross sections

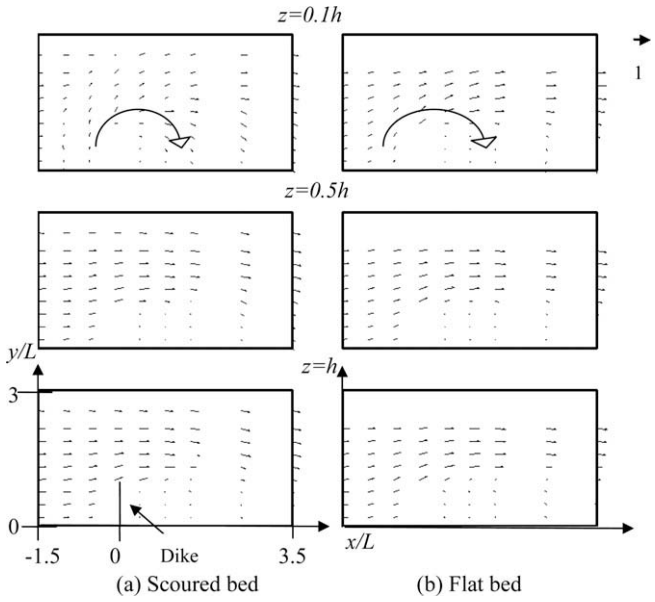

Fig. 5. Dimensionless velocity vector $(\bar{u}/u_0, \bar{v}/u_0)$ at different horizontal planes where $z = 0.1h$, $z = 0.5h$, and $z = h$.

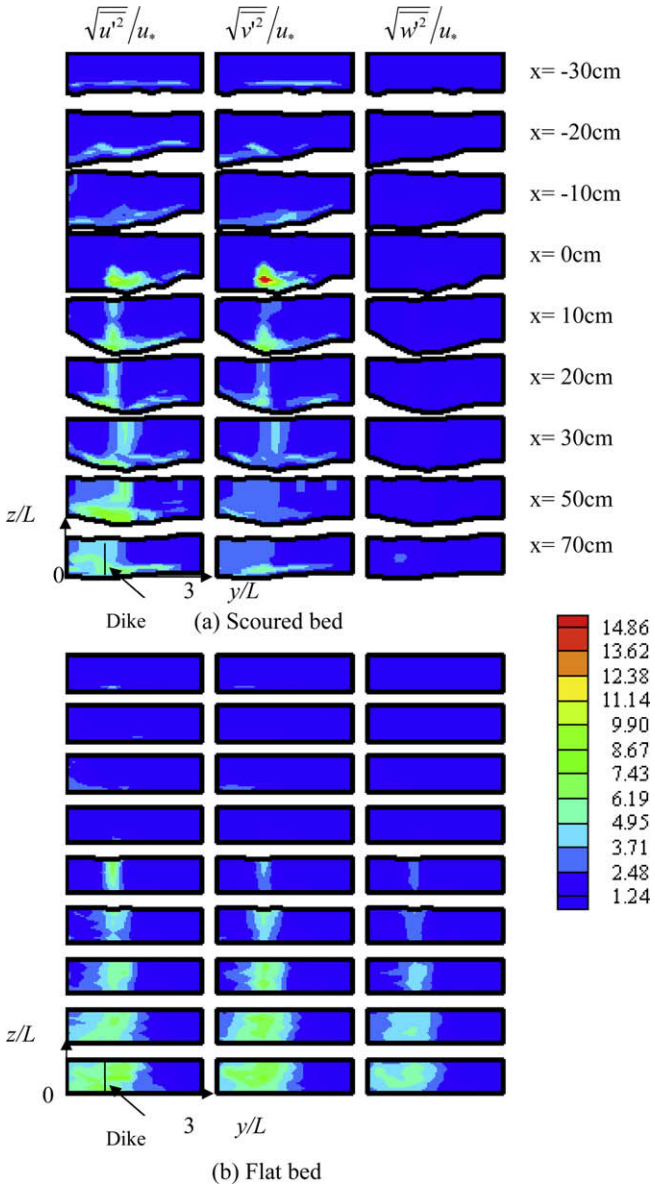

Fig. 6. Distribution of turbulent intensities $\sqrt{\overline{u'^2}}/u_*, \sqrt{\overline{v'^2}}/u_*$ and $\sqrt{\overline{w'^2}}/u_*$ at various cross sections for scoured and flat bed surfaces.

were shown in Fig. 6. In the flat bed, the turbulent intensities in three directions are nearly the same with a similar distribution. Turbulent intensities increase as the distance from the dike increases, while the largest turbulent intensity occurred at the center of each section.

After local scour reaches the asymptote state, the distributions of $\sqrt{\overline{v'^2}}$ and $\sqrt{\overline{w'^2}}$ are very similar to that of $\sqrt{\overline{u'^2}}$. The magnitude of $\sqrt{\overline{v'^2}}$ is larger than that of $\sqrt{\overline{u'^2}}$, and the magnitude of $\sqrt{\overline{w'^2}}$ is smaller than both. The magnitudes of $\sqrt{\overline{v'^2}}$ and $\sqrt{\overline{u'^2}}$ were increased at the dike tip in the scoured bed, but no noticeable increment was observed in the flat bed. At the contraction section, the turbulence intensities are the largest where $\sqrt{\overline{u'^2}}$ has nearly the same magnitude as u_0, while $\sqrt{\overline{v'^2}}$ is 1.65 times u_0. Downstream of the dike, the dimensionless $\sqrt{\overline{u'^2}}/u_*$ is larger than that in the flat bed. The increase of $\sqrt{\overline{v'^2}}$ in the local scour zone is not as apparent as that of $\sqrt{\overline{u'^2}}$. The turbulence intensity, $\sqrt{\overline{w'^2}}$, has increased in the area immediately above the bed upstream of the dike in the scour

hole, while there is limited increase near the right-hand side wall in the flat bed. While downstream of the dike, $\sqrt{\overline{w'^2}}$ has increased in the primary flow zone, and reduced in the flow recirculation zone.

3.4. Reynolds stresses

Since turbulent bursts were the dominant mechanism that entrains and transports sediment [6]. Fig. 7 showed Reynolds stresses produced by turbulent bursts. The magnitudes of $-\rho\overline{v'w'}$ and $-\rho\overline{u'w'}$ are much smaller than those of $-\rho\overline{u'v'}$. The change in signs means the magnitudes of velocity fluctuation in the streamwise and vertical direction are larger than those in the transversal. Consequently ejections and sweeps event are dominant [17].

As to $-\overline{u'w'}/u_*^2$, downstream of the dike, the sign of $-\overline{u'w'}/u_*^2$ changes from positive to negative as flow passes through the dike. Both the magnitude and probability of $-\overline{u'w'}/u_*^2$ are increasing, except for the primary flow zone. $-\overline{u'w'}/u_*^2$ in cross sections upstream of the dike are positive with larger values near the bed. Furthermore Reynolds stress $-\overline{u'w'}/u_*^2$ near the bed at sections upstream of the dike is less important than the corresponding turbulent intensity. Downstream of the dike, $-\overline{u'v'}/u_*^2$ are positive having a large magnitude. While upstream of the dike, the magnitude of negative $-\overline{u'v'}/u_*^2$ is relative larger than the positive one. The Reynolds stress $-\overline{u'v'}/u_*^2$ along the separation region is less important than the corresponding turbulent intensity because $-\overline{u'v'}/u_*^2$ is less than unity. Positive $-\overline{v'w'}/u_*^2$ indicated that either ejection or sweeps contributed more to Reynolds stresses than the negative ones. Nelson et al. [27] showed that fluctuations with high magnitudes and low time frequencies are important in the entrainment and movement of sediment, but not to the degree that those with higher frequencies can be neglected.

For the flat bed case, Reynolds stresses, $-\rho\overline{u'v'}$, $-\rho\overline{v'w'}$ and $-\rho\overline{u'w'}$, at cross sections downstream of the dike, gradually increases their magnitudes as the distance from the dike increases. Reynolds stress, $-\rho\overline{v'w'}$, is positive at sections upstream of the dike, and the stress in the recirculation zone changes to negative when it proceeds to cross sections downstream of the dike. As to $-\rho\overline{u'w'}$, the distribution of Reynolds stress is almost the same as that of $-\rho\overline{v'w'}$.

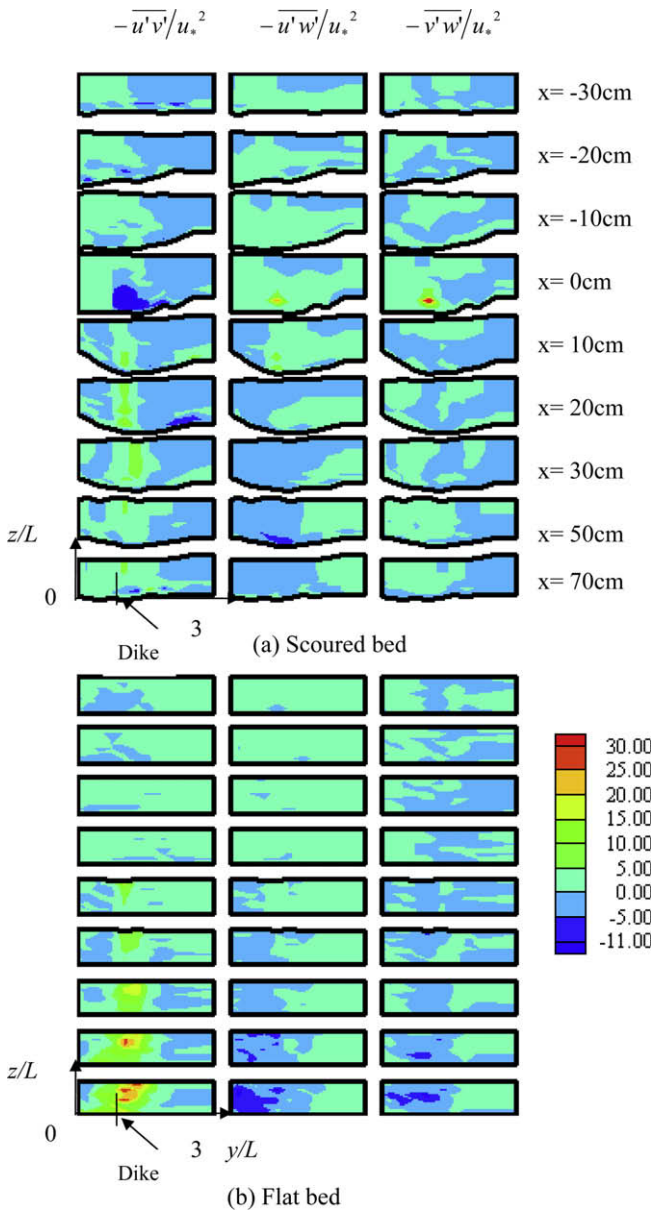

Fig. 7. Distribution of dimensionless Reynolds stresses at various cross sections $-\overline{u'v'}/u_*^2$, $-\overline{u'w'}/u_*^2$ and $-\overline{v'w'}/u_*^2$.

3.5. Normal stresses

The dimensionless normal stress $-\rho\overline{u'u'}/\rho u_*^2$ is the ratio of turbulence intensity to the friction velocity (u_*), so does $-\rho\overline{v'v'}/\rho u_*^2$ and $-\rho\overline{w'w'}/\rho u_*^2$. Fig. 8 showed the distributions of normal stress near the bed in both runs. The distributions of $-\rho\overline{u'u'}$ and $-\rho\overline{v'v'}$ are similar and their magnitudes are nearly the same near the bed in the flat bed case, but the magnitude of $-\rho\overline{w'w'}$ is smaller. But near the bottom of the scoured bed, the magnitude of $-\rho\overline{w'w'}$ is very small, while $-\rho\overline{u'u'}$ is very large within a small zone. Among three normal stresses, $-\rho\overline{u'u'}$, $-\rho\overline{v'v'}$, and $-\rho\overline{w'w'}$ all contributed to erosion around the dike tip, and $-\rho\overline{w'w'}$ is likely to contribute the most to the erosion upstream of the dike, and $-\rho\overline{u'u'}$ and $-\rho\overline{v'v'}$ become more important for the erosion as the local scour develops.

3.6. Bed Shear Stress

Bed-shear stress is still commonly used for estimating sediment transport rate in non-uniform unsteady flows [10]. If using the near-bed Reynolds stresses to approximate bed-shear stress, τ_b, the mathematical equation in [10] is $\tau_b = \sqrt{(\tau_b^x)^2 + (\tau_b^y)^2}$ in which $\tau_b^x = -\rho(\overline{w'u'} + \overline{v'u'})|_{bed}$ and $\tau_b^y = -\rho(\overline{w'v'} + \overline{v'u'})|_{bed}$, ρ = mass density of water. The bed-shear stress τ_b can be expressed in dimensionless form as $\widehat{\tau}_b = \tau_b/\tau_0$, where τ_0 = bed-shear stress of approaching flow.

In the scoured bed, bed shear stress at the dike section, $x/L = 0$, is the largest, which is also the deepest location in the scour hole. This coincidence verifies that the largest Reynolds stresses resulted in the most erosion. Three stripes of large bed shear stress are shown in Fig. 9. One originates from upstream of the dike, and curve along the edge of the scour hole. The second one starts from the dike tip and extends towards downstream. The third one initiates where erosion begins in the lee of the dike, and then it extends along the right side wall to the downstream. Ejections and sweeps are dominant burst events within these strips that contributed positively to the mean bed shear stress [27]. The ridge of each strip has the largest shear stress. Fan et al. [18] concluded that larger sized sediment particles damped more fluid turbulence than the smaller ones. As a result sediment at the ridge of each strip is relatively small, and the sediments at both sides are coarser. The

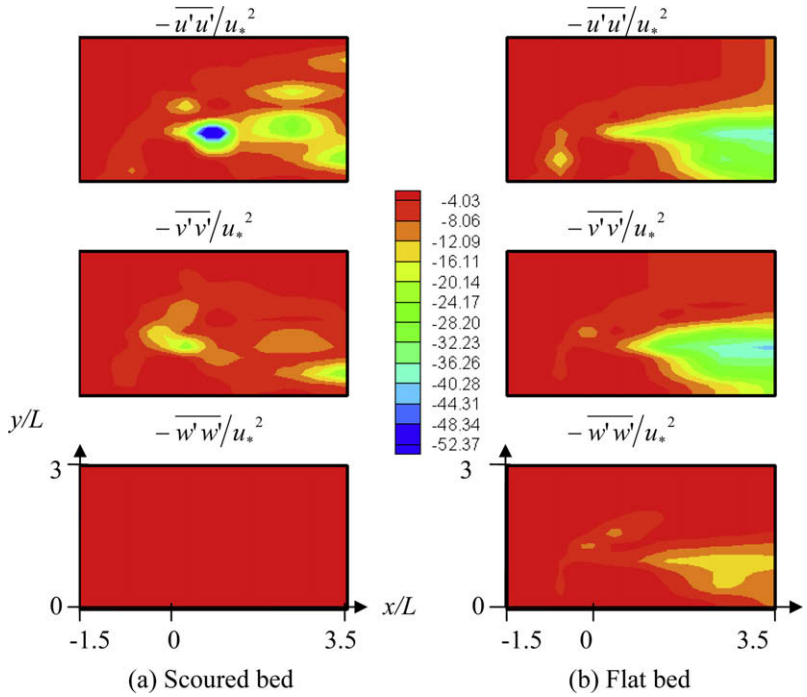

Fig. 8. Distributions of near-bed dimensionless Reynolds stresses $-\overline{u'u'}/u_*^2$, $-\overline{v'v'}/u_*^2$ and $-\overline{w'w'}/u_*^2$ ($z = 0$ cm).

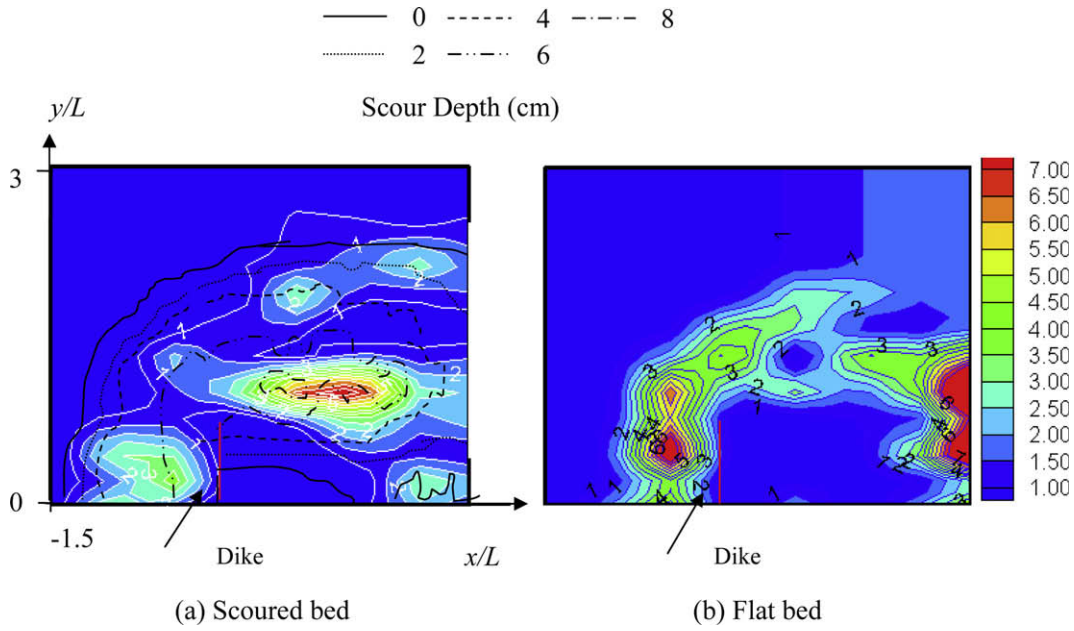

Fig. 9. Distributions of dimensionless bed-shear stresses $\widehat{\tau}_b = \tau_b/\tau_0$.

magnitudes of bed shear stress in the scoured bed are larger than those in the flat bed, especially at the maximum scoured depth. Bed shear stress in the flat bed case does not show stripes, and the dominant ejections and sweeps events occurred further downstream rather than at the dike tip. A high shear stress zone was shown in Fig. 9 that attributes to increased turbulence activities at the end of recirculation zone.

4. Discussion

A practical interest in the turbulent flow field around a spur dike is the need to accurately predict location and geometry (e.g. size, depth) of scour zone. In alluvial channel beds composed of primarily of sand and gravels, scour is often developed because of imbalance in sediment transport, especially bed load. Because bed material is directly exposed to shear stress acting on the bed surface, the rate of bed-load transport is proportional to bed-shear stress. Fine sand, silt, and clay are transported as suspended sediment in a water column and settle where the turbulence intensity is weak.

Experimental results from the present study showed the maximum shear stress occurred at the upstream side of the dike when the bed is non-erodible, but the deepest scour depth locates at the downstream of dike tip coinciding with the maximum shear stresses. The components of $-\rho\overline{u'w'}$ and $-\rho\overline{v'w'}$ Reynolds stress shown

in Fig. 7 contributed to the increase of bed-shear stresses in the scour zone, while the $-\rho\overline{u'v'}$ component is responsible for the high shear stress at the dike upstream side when bed surface is fixed. This shift of high bed-shear stress from the upstream to the downstream of the dike enabled the scour of mobile bed surface at the upstream side of the dike and gradually stretches to the downstream. The progression of scour zone follows the path of the horseshoe vorticies formed around the dike. McCoy et al. [24] applied large eddy simulation model and found that the high turbulent intensity and bed-shear stresses are produced by the necklace vorticies in the horseshoe vorticies region. As the vorticies transported to the downstream, loose bed material are entrained and transported in the zone of shear stress greater than the critical shear stresses of individual sized particles. This progressing of scouring zone was also observed in large flume experiments to test riprap-apron performance [25].

Although a certain size of particle may not be entrained at the upstream uniform flow reach, the same sized particles can be transported due to increased bed shear stresses near the dike. This mobile-bed laboratory experiment of sediment mixture showed that the coarse gravels, immobile at the upstream reach, was observed transporting around the dike tip due to increased shear stress and selective sediment transport. The scouring finally reached equilibrium when the remaining bed-load particles were too large to be entrained by bed shear stresses. The resultant scour hole was covered with particles of very coarse gravel, while the recirculation zone had aggraded with fine-suspended sediment shown in Fig. 2b. For uniformly sized material, the scouring hole will evolve to a maximum depth until the bed shear stresses are smaller than the critical shear stresses of a single grain-sized material. In the case of non-uniform material, the surface material covering the scour hole are coarser than the substrate material, so that the scour hole will not be as deep as the one formed in a mobile bed of uniform bed material.

5. Conclusions

Mean flow and turbulence fields around a spur dike in a flat and a scoured bed surface were analyzed. As for the scoured bed, flow separation zone in the lee of the dike was shortened. The mean streamwise velocity has been reduced, but both the lateral and vertical mean velocities are increased. In particular the turbulent intensity $\sqrt{\overline{w'^2}}$ near the bed has increased so much that the Reynolds stress $-\rho\overline{u'w'}$ and $-\rho\overline{u'w'}$ are the primary contributions of high bed shear stresses in the scour zone. As to non-erodible bed surface, $-\rho\overline{u'v'}$ is the major contributor of high shear stress at the upstream side of the dike.

Differences of shear stress and Reynolds stresses distributions showed that the scour is initiated at the dike upstream side and advance in the zone of high shear stress induced by horseshoe vorticies. The maximum scour depth occurred where the bed shear stress is maximum. For both non-erodible and erodible bed surface, the maximum bed shear stress is about 6 to 8 times of that of the approaching flow. Therefore, local scour will develop around a dike even though the approaching flow shear stress is less than the critical shear stress of bed material. With more computational models capable of simulating fine scaled turbulence eddies, the accurate prediction of local scour around a dike require direct simulations of turbulence structure.

Acknowledgements

The authors are grateful for research funding provided by NSF CAREER Award EAR-314630 and the Army Research Office under the proposal number 52326EV. This project is also in collaboration with the State Key Laboratory of Hydroscience and Engineering at Tsinghua University.

References

[1] Adrian RJ, Christensen KT, Liu Z-C. Analysis and interpretation of instantaneous turbulent velocity fields. Exp Fluids 2000;29:275–90.
[2] Azinfar H, Kells JA. Backwater prediction due to the blockage caused by a single, submerged spur dike in an open channel. J Hydraul Eng 2008;134(8):1153–7.
[3] Balachandar R, Bhuiyan F. Higher-order momentums of velocity fluctuations in an open-channel flow with large bottom roughness. J Hydraul Eng 2007;133(1):77–87.
[4] Balachandar R, Patel VC. Rough wall boundary layer on plates in open channels. J Hydraul Eng 2002;128(10):947–51.
[5] Blanckaert K, McLelland SJ. Simultaneous measurements with 3D PIV and acoustic Doppler velocity profiler. In: Proceedings of 33rd international association of hydraulic research congress, August, Vancouver, Canada; 2009.
[6] Bey A, Faruque MAA, Balachandar R. Two-dimensional scour hole problem: role of fluid structures. J Hydraul Eng 2007;133(4):414–30.
[7] Chrisohoides A, Sotiropoulos F, Sturm TW. Coherent structures in flat-bed abutment flow: computational fluid dynamics simulations and experiments. J Hydraul Eng 2003;129(3):177–86.
[8] Clifford NJ, McClatchey J, French JR. Measurements of turbulence in the benthic boundary layer over a gravel bed and comparison between acoustic measurements and predictions of the bed-load transport of marine gravels. Sedimentology 1991;38:161–71.
[9] Cuthbertson AJS, Ervine DA. Experimental study of fine particle settling in turbulent open channel flows over rough porous beds. J Hydraul Eng 2005;133(8):905–16.
[10] Dey S, Barbhuiya AK. Time variation of scour at abutments. J Hydraul Eng 2005;131(1):11–23.
[11] Dey S, Barbhuiya AK. Velocity and turbulent in a scour hole at a vertical-wall abutment. Flow Meas Instrum 2006;17:13–21.
[12] Dey Subhasish, Raikar Rajkumar V. Characteristics of horseshoe vortex in developing scour holes at piers. J Hydraul Eng 2007;133(4):399–413.
[13] Duan JG, Wang SSY, Jia Y. The application of the enhanced CCHE2D model to study the alluvial channel migration processes. J Hydraul Res 2001;39(5):469–80.
[14] Duan JG. Simulation of flow and mass dispersion in meandering channels. J Hydraul Eng 2004:566–76.
[15] Duan JG, Julien PY. Numerical simulation of the inception of meandering channel. Earth Surf Process Landforms 2005;30:1093–110.
[16] Duan JG, Nanda SK. Two-dimensional depth-averaged model simulation of suspended sediment concentration distribution in a groyne field. J Hydrol 2006. doi:10.1016/j.jhydrol.2005.11.055.
[17] Duan J, He L, Wang GQ, Fu XD. Turbulent burst around experimental spur dike. J Hydraul Eng 2009.
[18] Fan JR, Shi JM, Zheng YQ, Cen KF. The effect of particles on fluid turbulence in a turbulent boundary layer over a cylinder. Acta Mech Sinica 1997;13(1):36–43.
[19] Jia Y, Scott S, Xu Y, Huang S, Wang SY. Three-dimensional numerical simulation and analysis of flows around a submerged weir in a channel bendway. J Hydraul Eng 2005;131(8):682–93.
[20] Huai WH, Zeng YH, Xu ZG, Yang ZH. Three-layer model for vertical velocity distribution in open channel flow with submerged rigid vegetation. Adv Water Resour 2009;32(4):487–92.
[21] Koken M, Constantinescu G. An investigation of the flow and scour mechanisms around isolated spur dikes in a shallow open channel: 1. Conditions corresponding to the initiation of the erosion and deposition process. Water Resour Res 2008;44:W08406. doi:10.1029/2007WR006489.
[22] Kuhnle RA, Alonso CV, Shields Jr FD. Geometry of scour holes associated with 90° spur dikes. J Hydraul Eng 1999;125(9):972–8.
[23] Kuhnle RA, Jia Y, Alonso CV. Measured and simulated flow near a submerged spur dike. J Hydraul Eng 2008;134(7):916–24.
[24] McCoy A, Constantinescu G, Weber L. A numerical investigation of coherent structures and mass exchange processes in channel flow with two lateral submerged groynes. Water Resour Res 2007;43:W05445. doi:10.1029/2006WR005267.
[25] Morales R, Ettema R, Barkdoll B. Large-scale flume tests of riprap-apron performance at a bridge abutment on a floodplain. J Hydraul Eng 2008;134(6):800–9.
[26] Nagata N, Hosoda T, Nakata T, Muramoto Y. Three-dimensional numerical model for flow and bed deformation around river hydraulic structures. J Hydraul Eng 2005;131(12):1074–87.
[27] Nelson JM, Shreve RL, Mclean SR, Drake TG. Role of near-bed turbulence structure in bed load transport and bed form mechanics. Water Resour Res 1995;31(8):2071–86.
[28] Nezu I, Nakagawa H. Turbulent in open-channel flow. IAHR monograph series. Rotterdam, The Netherlands: Balkema, Taylor & Francis; 1993.
[29] Papanicolaou AN, Diplas P, Dancey CL, Balakrishnan M. Surface roughness effects in near-bed turbulence: implications to sediment entrainment. J Eng Mech 2001;127(3):211–8.
[30] Radice A, Ballio F, Nikora V. On statistical properties of bed load sediment concentration. Water Resour Res 2009;45:W06501. doi:10.1029/2008WR007192.

[31] Salaheldin TM, Imran J, Chaudhry MH. Numerical modeling of three-dimensional flow field around circular piers. J Hydraul Eng, ASCE 2004;130(2):91–100.
[32] Ojha Satya P, Mazumder BS. Turbulence characteristics of flow region over a series of 2-D dune shaped structures. Adv Water Resour 2008;31(3):561–76.
[33] Schmeeckle MW, Nelson JM, Shreve RL. Forces on stationary particles in near-bed turbulent flows. J Geophys Res 2007;112:F02003.
[34] Kim S-C, Friedrichs CT, Maa JP-Y, Wright LD. Estimating bottom stress in tidal boundary layer from acoustic Doppler velocimeter data. J Hydraul Eng 126(6):399–406.
[35] Sterk G, Jacobs AFG, Van BJH. The effect of turbulent flow structures on saltation sand transport in the atmospheric boundary layer. Earth Surf Process Landforms 1998;23:877–87.
[36] Thorne PD, Williams JJ, Heathershaw AD. In situ acoustic measurements of marine gravel threshold and transport. Sedimentology 1989;36:61–74.
[37] Thompson DM. The role of vortex shedding in the scour of pools. Adv Water Resour 2006;29:121–9.
[38] Wu FC, Jiang MR. Numerical investigation of the role of turbulent bursting in sediment entrainment. J Hydraul Eng 2007;133(3):329–34.